Reconstruction of 3D light distribution produced by cylindrical diffuser in deep tissues based on photoacoustic imaging

Wenming Xie (谢文明)[1,2,3], Yubin Liu (刘玉滨)[1,2,3], Zhifang Li (李志芳)[1,2,3], and Hui Li (李 晖)[1,2,3*]

[1]*Key Lab of OptoElectronic Science and Technology for Medicine, Ministry of Education*

[2]*Fujian Provincial Key Lab of Photonic Technology*

[3]*College of Photonic and Electronic Engineering, Fujian Normal University, Fuzhou, Fujian 350007, China*

[*]*Corresponding author: hli@fjnu.edu.cn*

Received December 16, 2013; accepted March 27, 2014; posted online April 30, 2014

Measurement of light distribution in biological tissue contributes to selecting strategy and optimizing dose for biomedical application. In this letter, a photoacoustic method combined with Monte Carlo simulation was used to estimate the three-dimensional light distribution in biological tissue. The light distribution was produced by a cylindrical diffuser which interposed into tissues. The light profiles obtained by the method were compared to those detected by photo diodes. The experimental results demonstrate the feasibility of this method. The approach can play a significant role for photo-dosimetry in biomedical phototherapy.

OCIS codes: 170.5120, 000.4430, 120.5240.

doi: 10.3788/COL201412.051702.

Cylindrical diffuser has its advantage because it could illuminate a larger volume of target tissue than conventional fibers by attaching diffusing ends. Cylindrical diffuser is widely applied in light therapies, such as photodynamic therapy, photo-thermal therapy, photocoagulation, *et al.*[1−3]. These therapy methods depend on optical and mechanical characteristics of the diffuser to a large extent. Moreover, the light emission profile of diffuser at distal end is dramatically influenced by many parameters in the producing process[4]. From a clinical point of view, an unknown light distribution in tissues would lead to an improper treatment or could be even worse. Therefore, it is important to know the light distribution and emission profile in their applications.

Although there are some methods to measure the light distribution by using a cylindrical diffuser in either air or turbid media[5−8], no method has been used in living tissues, especially for deep tissues. In general, a simulation method is often employed before surgery in order to predict the light distribution[6], in which a uniform illumination by the diffuser was generally assumed. However, this assumption is practically inaccurate, so the simulation results only serve as references and are not suitable for the practical therapy. Dimofte *et al.*[5] proposed an invasive method in which an optical fiber-based isotropic detector was used to measure light distribution in tissues through transparent plastic catheters, but its invasive procedure limits its practical applications. A video technique was introduced by Ripley *et al.*[9] to reconstruct the light emission profile of diffuser in phantom. But this method becomes very challenging and unreliable when the cylindrical diffuser was applied in deep tissues, such as the prostate, esophagus, etc. Thus, when a cylindrical diffuser in deep tissues is employed, a non-invasive and accurate method to detect the light distribution is desired for various clinic applications.

Photoacoustic imaging which offers a function imaging-with non-invasive, non-ionizing method[10,11] works as a promising technique because the technique overcomes not only the disadvantage of the weakening effect of optical imaging caused by strong scattering in tissues, but also the low contrast provided by ultrasound. Photoacoustic signal has such a high sensitivity to the absorption of tissues that the fundamental quantity was to be determined by chromophores concentration. Therefore, a quantitative estimation of parameters of physiological should be derived, such as absorption coefficient, hemoglobin oxygen saturation, etc.

In this letter, we proposed an approach which combined a photoacoustic imaging with Monte Carlo simulation to characterize the three-dimensional (3D) light profile of cylindrical diffuser in tissues. First of all, to demonstrate the feasibility of accurate measurement by photoacoustic imaging, we compared the results of light profile which are obtained by the photoacoustic method and photo diode, respectively. Secondly, the light profile of cylindrical diffuser applied in phantom and tissues *in vitro* was imaged. Then, the fiber was positioned and the function of light profile of diffuser was derived by fitting. Finally, we reconstructed the 3D light distribution of cylindrical diffuser in tissues through the fitting function and Monte Carlo simulation.

In principle of photoacoustic imaging, the pressure is linearly related to the absorbed light energy as written by

$$P_0(r) = \Gamma \mu_{\mathrm{a}} F_1(\mathrm{r}), \tag{1}$$

where Γ is the dimensionless Gruneisen parameter; μ_{a} is the optical absorption coefficient and $F_1(\mathrm{r})$ is the optical fluence. Equation (1) has been used to estimate the optical parameters of tissue[12]. Conversely, the fluence ($F_1(\mathrm{r})$) could be obtained in condition of knowing the absorbing coefficient and pressure ($P_0(\mathrm{r})$). So the

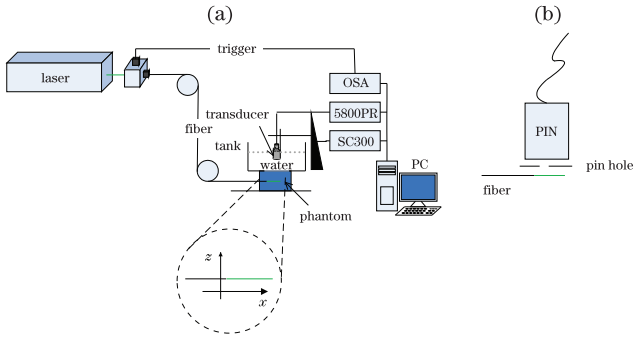

Fig. 1. Schemetric of systems. (a) System of photoacoustic scanning. (b) System of photo-diode scanning.

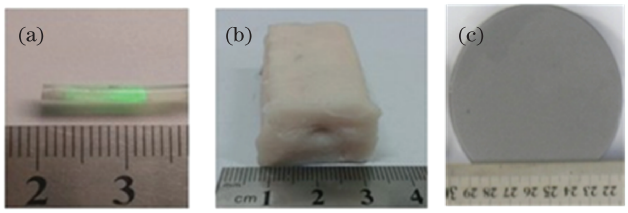

Fig. 2. (a) Photo of light profile of the commercial cylinder diffuser (distal end). The rigid diffuser distal ends are 10 mm in length with 1000-μm diameter. (b) A swine fat *in vitro* with a volume of 20 × 15 × 50 (mm). (c) A photo of the simulated phantom with 100-mm diameter, 25-mm thickness.

fluence is proportional to the local pressure (P_0(r)). In order to estimate the fluence on the interface of tissue, the calibration was operated before measurement. In other words, the related parameters of physiological stated should be obtained first by other methods.

The schematic of system was illustrated in Fig. 1(a). The System was consisted of a short pulse laser, a cylindrical diffuser and a focused transducer, etc. The laser beam with 532-nm wavelength, 6-ns pulse width and 10-Hz pulse repetition was generated by an Nd:YAG laser (Surelite I-10, Continuum). The laser beams were coupled into the fiber with a cylindrical diffuser tip. The end tip was inserted into the phantom to excite the photoacoustic signals. The focal transducer (V381, Panametrics-NDT, USA) with 3.5-M central frequency, 60-mm focus length, and 3.68 F-number, was used to collect the time-resolved signals. The transducer was immobilized on a stage. The axis of the transducer was in the vertical plane of the fiber. The stage was moved by an xy-stage which was driven preciously by a computer-controlled step motor for scanning along axial x direction. The time-resolved photoacoustic signals were amplified by an amplifier (PR5800, Panametrics-NDT, USA) and monitored via a digital oscilloscope (TDS3054c, Tektronix, USA). The photoacoustic signals, which were averaged sixteen times in order to eliminate the serious stochastic noise, were acquired by a personal computer.

A diffuser is 1 cm in length and 1 mm in diameter as shown in the Fig. 2(a). In order to confirm the feasibility of the photoacoustic method, the fiber was profiled in air by mentioned photoacoustic system and a photodiode (ET-2030, Electro-Optics Technology) with a pinhole (0.5-mm diameter) as described in Fig. 1. The photodiode with pinhole was moved along the axial x to obtain the light profile in air. Photoacoustic system as shown in Fig. 1 should follow the following steps. Firstly, the fiber was coated with a thin layer of ink and contacted to the water tank with a hole at the bottom, where a piece of clear polyethylene film between the water and the fiber was used to seal the hole in air. Meanwhile, the fiber was positioned in the focused volume of the transducer. The focused transducer immerged in water was used to scan along the axial x to detect the photoacoustic signals. Secondly, a simulated phantom (as shown in Fig. 2(c)) and a swine fat *in vitro* were used to characterize the actual performance of the system. The simulated phantom was made with 300-ml distilled water, 6-g agar powder, and 10 ml Intralipid-20%. The phantom of fat *in vitro* was illustrated in the Fig. 2. The volume was $20\times15\times50$ (mm) with a 1-mm diameter hole. The diffusing tip was placed inside the phantoms through the hole to excite the photoacoustic signals. Phantom targets were placed under the tank as shown in Fig. 1. Finally, the relative fluence rate was indirectly measured with the transducer which was moved along the parallel direction.

The light output at the same diffusing tip was collected and digitized by the photodiode with a pinhole and aforementioned photoacoustic system, respectively. Fig. 3(a) shows the light distribution of the diffusing tip with an active length of 1 cm by scanning along longitudinal direction with the photodiode. The curve in the Fig. 3(a) steeply rose at the proximal of the diffuser, and then declined gradually to the distal end. Figure 3(b) shows the result of the same fiber which was detected through the photoacoustic method. The amplitude of photoacoustic signals increased gradually, and then held, finally descended to the distal end of diffuser. Even though

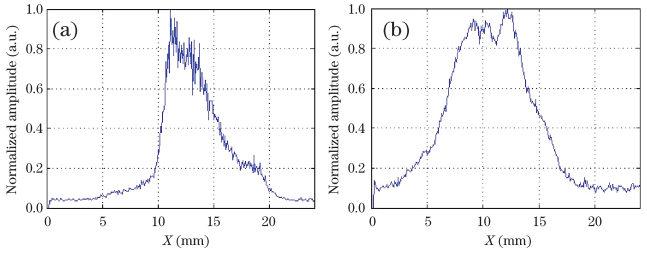

Fig. 3. (a) Profile of normalized voltage of photodiode along axial x. (b) Profile of normalized amplitude of the photoacoustic signal along axial x.

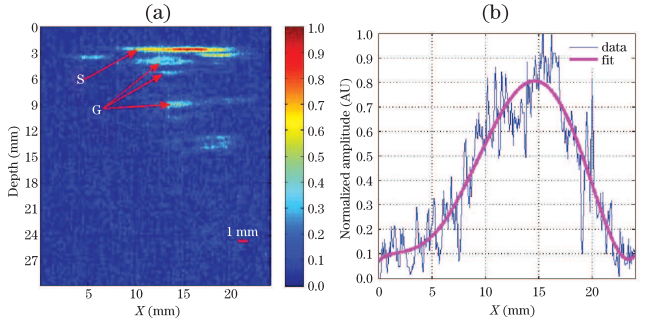

Fig. 4. (a) Sagittal intensity distribution of photoacoustic corresponding to scanning phantom with diffuser along axial x; (b) Amplitude profile of photoacoustic signals corresponding to the position pointed by arrow in (a) along axial x. 4^{th} degree polynomial is used as a fitting function to fit the raw data. Fitting curve shows as the purple line.

the radiation of diffuser and different detected methods caused the photoacoustic signals at the central section of diffuse tip to increase, Figs. 3(a) and 3(b) still showed the similar trends at the diffuse tip.

Figure 4(a) depicts the cross-section intensity imaging for absorption in the simulated phantom. The distribution of absorption at interface was corresponding to the inner surface of phantom catching photons delivered from the cylindrical diffusing tip of fiber to generate the photoacoustic signals as pointed by arrow S. What pointed by arrow G was produced by the resonance in the inner wall. Figure 4(b) shows the normalized amplitude of photoacoustic signals corresponding to the length of about 15.4 mm. And the 4th degree polynomial was employed as a fitting function to fit the raw data. The purple line is the fitting curve.

Figure 5(a) shows a cross-section photoacoustic image of swine fat *in vitro* when the diffuser was inserted into the phantom to deliver light. What the arrow S pointed is the distribution of absorption at the interface. It was shown in the Fig. 5(b) that the normalized amplitude of photoacoustic signals corresponding to what the position arrow S pointed along axial x. Meanwhile, the aforementioned function, 4th degree polynomial, was employed too. The data were fitted shown as the purple curve.

Parameters of fitting function corresponding to light distribution at interface were obtained by fitting the curve in Fig. 5(b). Through combining the known absorption coefficient of phantom and maximum amplitudes of photoacoustic signals and Eq. (1), estimated light distribution of diffuser emission could be reconstructed by the fitting function. In Monte Carlo simulations, the distribution of light source could be convoluted by the fitting function. As for the photon incident direction, it can be considered as an isotropic point. The tissue sample with μ_a= 0.1 cm^{-1}[13], μ_s=100 cm^{-1}, g = 0.9, and n = 1.395, was assumed. A typical two-dimensional and 3D fluence rate maps were shown in Fig. 6.

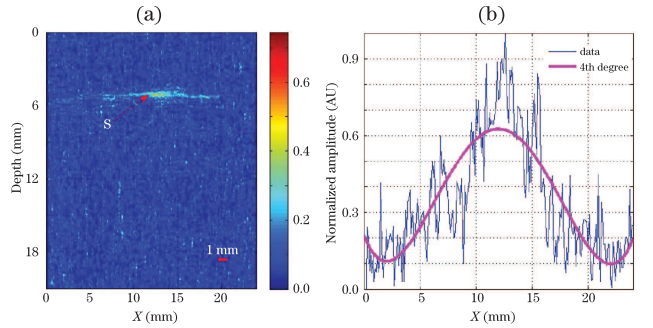

Fig. 5. (a) Sagittal intensity distribution of photoacoustic corresponding to scanning fat of swine with diffuser along axial x; (b) Amplitude profile of photoacoustic signals corresponding to the position pointed by arrow in (a) along axial x. The purple line is the fitting curve.

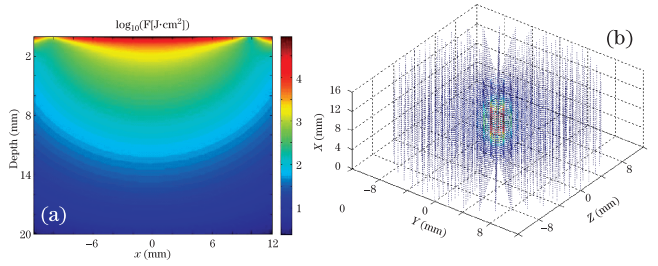

Fig. 6. Rendered fluence distribution map of cylindrical diffusers in vitro tissue. (a) Cross-section map of diffuser at one side; (b) 3D distribution around 1-cm cylindrical diffuser in vitro tissue.

The curve in Fig. 3(b) was fairly consistent changed as it was shown in the Fig. 3(a). The curves rose at the proximal, and then declined gradually to the distal end. The result agreed with the measurement produced by photodiode in air as shown in Fig. 3(a). But the strongly forward radiation pattern of diffuser lead to the forward shift and broadening the maximum fluence rate on the inner wall of phantom[14]. In addition, high scattering property of biological tissue and some leakage of light outside the intended diffusing area lead to a wider distribution of incident light on the interface than those of the diffuser. The size of beam diameter of focal transducer might affect it to a certain extent. The transversal resolution of our system is about 2 mm. The area of light illumination covers around 10 mm and the fitted distribution of light is rather smooth. So it is reasonably based on our system and Monte Carlo simulation. Of course, the high resolution system should be more accurate than the low one, but the depth would be sacrificed.

Both Figs. 4 and 5 show the performance of the system for the simulated phantom and tissue in vitro. The position of fiber could be easy to identify in the graph. In addition, an artifact to which the arrow G pointed in Fig. 4(a) was generated by photoacoustic signals which resonated in the inner hollow. Since there was tightly contact between fiber and phantom of vitro tissue, the phenomenon was not observed in Fig. 5.

According to the Eq. (1) and calibration, the curve in Figs. 3(b), 4, and 5 not only showed the profile of normalized amplitude of photoacoustic signals, but also depicted the distribution of light fluence on the interface of tissue along the x axial. Thus, we could fit the curve in Fig. 5(b) to get the function of related distribution of light. Finally, through combining the function with Monte Carlo simulations, the 3D distribution of light in tissue could be reconstructed as shown in Fig 6.

At present, some optical detectors like photodiode, isotropic detector, CCD/video camera[5,9], were employed to quantify the light distribution in soft tissues. But with these detectors, it is hard to measure the light profile in deep tissues by strong scattering. And invasiveness could destroy the structure of tissues. For numeric calculation, the light distribution was unknown. From the results of the measurement above, there were quite different ones that the light profile did on inner wall in tissues versus in air. The presented approach which combined photoacoustic imaging with Monte Carlo overcome these obstacles with non-invasiveness and deeper imaging depth. And 3D light distribution was reconstructed for the diffuser radiation in the tissue. The Results of measurement of light distribution in tissues might provide a reference of dose for photodynamic therapy or photo-thermal therapy, photocoagulation, etc.

In conclusion, we proposed a photoacoustic method for the estimation and reconstruction of 3D light distribution produced by the cylindrical diffuser in biological

tissue. The results demonstrated the feasibility of the approach. It overcomes the short hand of Monte Carlo simulations which original light profile in tissue was unknown. Non-invasive and deep depth of detection was the typical character of the method which could be relatively easy to be employed for clinical use.

This work was supported by the National Natural Science Foundation of China (No. 61178089/81201124), and in part by the Natural Science Foundation of Fujian Province (No. 2011Y0019).

References

1. X. Liang, K. Wang, and T. Zhu, Phys Med. Biol. **10,** 3461 (2013).
2. A. Rendon, J. C. Beck, and L. Lilge, Phys. Med. Biol. **53,** 1131 (2008).
3. M. Arnfield, S. Gonzalez, M. Mcphee, J. Tulip, and P. Lea, Laser Surg. Med. **2,** 150 (1986).
4. W. Small, P. R. Buckley, T. S. Wilson, J. M. Loge, K. D. Maitland, and D. J. Maitland, J Biomed. Opt. **13,** 024018 (2008).
5. A. Dimofte, J. C. Finlay, X. Liang, and T. Zhu, Phys. Med. Biol. **57,** 6025 (2012).
6. T. M. Baran, and T. H. Foster, J Biomed. Opt. **16,** 085003 (2011).
7. P. M. Ripley, T. N. Mills, and J. A. S. Brookes, Laser Med. Sci. **14,** 67 (1999).
8. R. L. Kozodoy, S. L. Lundahl, D. Bell, and J. A. Harrington, Appl. Opt. **33,** 6674 (1994).
9. P. M. Ripley, T. N. Mills, and J. A. S. Brookes, Laser Med. Sci. **14,** 67 (1999).
10. Y. Gao, Y. Deng, X. Dong, H. Wang, Z. Deng, X. Yang, Y. Liu, H. Gong, and Q. Luo, Chin. Opt. Lett. **06,** 29 (2012).
11. S. Ye, J. Yang, J. Xi, Q. Ren, and C. Li, Chin. Opt. Lett. **12,** 52 (2012).
12. Z. Li, H. Li, Z. Zeng, W. Xie, and W. Chen, J. Biomed. Opt. **17,** 061216 (2012).
13. R. J. Zemp, J. Ranasinghesagara, Y. Jiang, X. Chen, and K. Mathewson, SPIE **7177,** 71770Q (2009).
14. L. H. P. Murrer, J. P. A. Marijnissen, and W. M. Star, Phys. Med. Biol. **41,** 951 (1996).